

# Hawking radiation on the lattice as universal (Floquet) quench dynamics

Daan Maertens,<sup>1</sup> Nick Bultinck,<sup>2,1</sup> and Karel Van Acoleyen<sup>1</sup>

<sup>1</sup>*Department of Physics and Astronomy, University of Ghent, Krijgslaan 281, 9000 Gent, Belgium*

<sup>2</sup>*Rudolf Peierls Centre for Theoretical Physics, Parks Road, Oxford, OX1 3PU, UK*

We construct two free fermion lattice models exhibiting Hawking pair creation. Specifically, we consider the simplest case of a  $d=1+1$  massless Dirac fermion, for which the Hawking effect can be understood in terms of a quench of the uniform vacuum state with a non-uniform Hamiltonian that interfaces modes with opposite chirality. For both our models we find that additional modes arising from the lattice discretization play a crucial role, as they provide the bulk reservoir for the Hawking radiation: the Hawking pairs emerge from fermions deep inside the Fermi sea scattering off the effective black hole horizon. Our first model combines local hopping dynamics with a translation over one lattice site, and we find the resulting Floquet dynamics to realize a causal horizon, with fermions scattering from the region outside the horizon. For our second model, which relies on a purely local hopping Hamiltonian, we find the fermions to scatter from the inside. In both cases, for Hawking temperatures up to the inverse lattice spacing we numerically find the resulting Hawking spectrum to be in perfect agreement with the Fermi-Dirac quantum field theory prediction.

*Introduction* – In 1974, Hawking showed in a seminal paper that quantum effects cause black holes to emit thermal radiation [1]. This surprising and intriguing result was originally derived [2], and has since then mostly been discussed, in the framework of quantum field theory (QFT) in classical curved spacetime [3–5]. Following Hawking’s result, Unruh showed that a sonic horizon in a fluid will similarly emit thermal radiation [6]. This groundbreaking insight gave rise to the field of analogue gravity [7, 8], and since then different experimental platforms for observing analogue Hawking radiation have been put forward, including classical water waves [9], superfluid Helium [10], ion traps [11] and Bose-Einstein condensates [12], for which Steinhauer recently reported the actual detection of spontaneously emitted Hawking radiation [13]. Moreover, on the theoretical front there has been the realization that the analogue gravity models bypass the *trans-Planckian problem* [14–17]: where for the strictly relativistic QFT case, the Hawking radiation suspiciously relies on an infinite reservoir of arbitrary short distance near-horizon modes, it was shown that this is no longer the case for the Lorentz-violating analogue gravity models [15, 17–21].

In this work, we approach the phenomenon of Hawking radiation from a purely quantum many-body point of view. In contrast to previous works on Hawking radiation in analogue gravity, we consider lattice models with fermionic degrees of freedom (see also [22–27]). We also do not try to construct models that exactly emulate the behavior of a quantum field in a black hole spacetime. Instead, we aim to explain the Hawking effect entirely in terms of simple physical concepts associated with quantum many-body systems. In particular, we argue that to understand Hawking radiation, no knowledge of general relativity is required – it can be understood as a universal quantum dynamics phenomenon in many-body systems with gapless, linearly dispersing excitations.

In its most stripped down version, a (static) causal

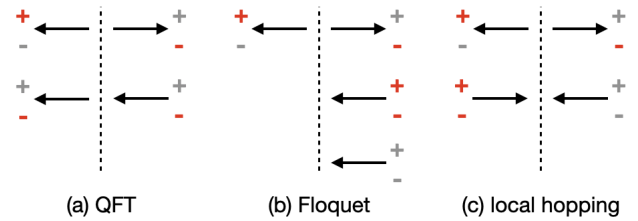


FIG. 1. The black hole horizon as a boundary between chirality-changing modes, with the inside of the (effective) black hole on the left. In all cases the right-mover outside becomes a left-mover on the inside (upper arrows). (a) For a massless Dirac fermion (QFT) the extra left-mover decouples and is unaltered across the horizon; (b) for the Floquet model, we have two additional left-moving modes (‘doublers’) on the outside; (c) for the local hopping model, we have a right-moving ‘doubler’ on the inside and a left-moving ‘doubler’ on the outside. The + (-) symbols give the occupation of the positive- (negative-) energy states, for the Minkowski groundstate (see text), with grey (red) denoting empty (filled) modes.

horizon for a free massless Dirac fermion is a boundary between a region with both a left- and right-moving mode (right of the horizon), and a region with two left-moving modes (left of the horizon). This is illustrated in Fig. 1 (a). The region ‘behind’ the horizon corresponds to the chiral region with two left movers. Particles behind the horizon can clearly never cross the horizon. Note that for concreteness, we have made a particular choice of horizon here – we could equally well have the horizon separate two right-movers from a left- and right-mover. In both cases, the Hawking effect is entirely due to the mode which changes its chirality upon crossing the horizon. In particular, as we discuss in more detail below, Hawking radiation occurs when the ground state of the Hamiltonian  $\hat{H}_0$ , which has a left- and right-mover everywhere, is evolved in time with a Hamiltonian which has a chirality-changing mode at the horizon. In the supplementary ma-

terial [28] we show that for a continuum Dirac fermion this quench process indeed produces thermal Hawking radiation with a temperature  $T_H = (2\pi k_B)^{-1} \hbar \partial_x v(x)|_{x=0}$ , where  $k_B$  is Boltzmann's constant,  $x = 0$  is the location of the horizon, and  $v(x)$  is the spatially-varying velocity of the chirality-changing mode.

The chiral nature of the region behind the horizon is a problem for lattice models, as the Nielsen-Ninomiya theorem states that every local lattice Hamiltonian has a zero net chirality [29]. To circumvent this problem, we adopt two different approaches. In the first, we discretize the time-evolution – turning the dynamics into a Floquet problem. In this case we are able to realize an exact causal horizon on the lattice, albeit at the price of going beyond the framework of local Hamiltonian time evolution. In the second approach, we study continuous time-evolution with a local lattice Hamiltonian which does not have a strict causal horizon, but does have a special point where *both* the left- and right-moving modes simultaneously change chirality (such that the net chirality is zero everywhere). For both models we find the Hawking effect in excellent agreement with the QFT results.

*Floquet quench dynamics* – We start by defining the ‘Minkowski’ Hamiltonian  $\hat{H}_0$ , which is translationally invariant and has a gapless left- and right-moving mode. It is given by a simple free fermion Hamiltonian describing electrons hopping on a 1D spatial lattice:  $\hat{H}_0 = \sum_{j=1}^N \frac{t}{2} (ic_{j+1}^\dagger c_j - ic_j^\dagger c_{j+1})$ , where  $c_j^\dagger, c_j$  satisfy the canonical fermion anti-commutation relations  $\{c_j^\dagger, c_{j'}\} = \delta_{j,j'}$  and  $\{c_j^\dagger, c_{j'}^\dagger\} = \{c_j, c_{j'}\} = 0$ . Its groundstate has all negative momentum modes occupied:  $|\psi_0\rangle = \prod_{-\pi/a < k < 0} \tilde{c}_k^\dagger |0\rangle$ , with  $\tilde{c}_k = \sum_j e^{-ikja} c_j$  and  $c_j |0\rangle = 0$ . The right-moving mode occurs at  $k = 0$ , and the left-moving mode at  $k = \pi/a$  ( $a$  is the lattice constant, and from now on,  $\hbar = 1$ ). The velocity of these modes is given by  $\pm v$  with  $v = at$ .

Next we define a Floquet time evolution operator  $U(\Delta t)$  with a static causal horizon. The Floquet unitary can be written as a product of two operators:

$$U(\Delta t) = \hat{T}_L e^{-i\Delta t \hat{H}}, \quad (1)$$

where  $\hat{T}_L c_j^\dagger \hat{T}_L^{-1} = c_{j-1}^\dagger$  (with  $c_0^\dagger = c_N^\dagger$ ) implements a translation to the left, and  $\hat{H} = \sum_{j=1}^N \frac{t_j + t_{j+1}}{4} (ic_{j+1}^\dagger c_j - ic_j^\dagger c_{j+1})$  is a generalization of  $\hat{H}_0$  which is not translationally invariant. The spatially-varying hopping strengths in  $\hat{H}$  are defined as  $t_j = t(ja)$ , where  $t(x)$  is a continuous function of position. Associated with  $t(x)$  we can define a corresponding velocity function  $v(x) = at(x)$ . Defining the intrinsic Floquet velocity as  $v_{Fl} = a/\Delta t$ , the velocity function satisfies  $v(x) > v_{Fl}$  for  $x_b < x < x_w$ , and  $v(x) < v_{Fl}$  for  $x < x_b$  and  $x > x_w$ , where  $x_b$  and  $x_w$  respectively denote the location of a black hole horizon ( $\partial_x v(x)|_{x=x_b} > 0$ ) and a white hole horizon ( $\partial_x v(x)|_{x=x_w} < 0$ ). Note that we are forced to simul-

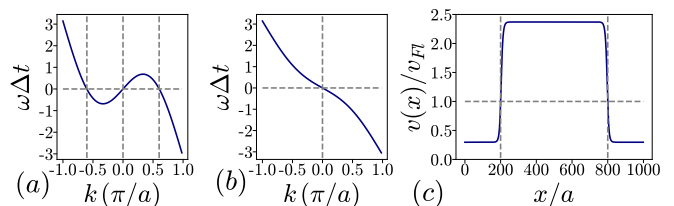


FIG. 2. (a)-(b) Floquet frequencies for spatially uniform  $t_j = t$ . In (a),  $v = at = 2v_{Fl}$ . This corresponds to the region outside the horizon. The vertical dashed lines show  $k = 0$  and  $k = \pm k^*$ . In (b),  $v = v_{Fl}/2$ . This corresponds to the region inside the horizon. (c) Example of  $v(x)$  with  $\kappa\Delta t = 0.1$ . (Eq. (53) in the supplementary material [28] with  $N = L/a = 1000$ ,  $W/a = 600$ ,  $b = 3$ , and  $\bar{\kappa}a = 0.1$ .) The locations of the black hole horizon  $x_b = 200a$  and white hole horizon  $x_w = 800a$  are indicated with dashed lines.

taneously introduce a black hole and a white hole horizon because of the periodic boundary conditions. In Fig. 2(c) we show an example of  $v(x)$  used in our numerics. From the properties of  $v(x)$ , it is intuitively clear why the Floquet unitary in Eq. (1) has a black hole horizon at  $x = x_b$ . During the first part of the Floquet time-evolution, a particle at position  $j$  can travel a distance  $v(ja)\Delta t$  to the right. After this initial time evolution, the Floquet unitary implements a translation to the left over one lattice constant  $a$ . If  $v(ja)\Delta t < a$ , or equivalently  $v(ja) < v_{Fl}$ , then every particle necessarily has a net displacement to the left during one Floquet time-step. This is true for particles behind the black hole horizon, corresponding to the region with  $ja < x_b$  and  $ja > x_w$ . The white hole horizon at  $x_w$  corresponds to a point from which particles can only escape, but not enter, the region behind the black hole horizon. In this work, we focus on the dynamics resulting from the black hole horizon, and from now on we will refer to the black hole horizon simply as the horizon, and the region  $x_b < ja < x_w$  as the region outside the horizon.

In Fig. 2, we plot the single-particle Floquet frequencies  $\omega$ , defined via the eigenvalue equation  $U(\Delta t)(\sum_j w_j^\omega c_j^\dagger)U(\Delta t)^\dagger = e^{-i\omega\Delta t}(\sum_j w_j^\omega c_j^\dagger)$ , as a function of momentum for the spatially uniform case where  $t_j = t$  is constant (such that  $\hat{H} = \hat{H}_0$ ). We plot  $\omega(k) = v \sin(ka)/a - kv_{Fl} \bmod 2\pi/\Delta t$  both for the case where  $v > v_{Fl}$  [Fig. 2 (a)], and the case where  $v < v_{Fl}$  [Fig. 2 (b)]. The former corresponds to the region outside the region, and the latter to the region behind the horizon. Note that because Floquet frequencies are only defined mod  $2\pi/\Delta t$ ,  $\omega(k)$  is a continuous function of  $k$  over the entire Brillouin zone. The gapless modes of  $\hat{H}_0$  correspond to the Floquet frequencies  $\omega = 0$  and  $\omega = \pi/\Delta t$ . The gapless mode at  $k = 0$  changes from right-moving on the outside of the horizon to left-moving on the inside. Note that outside the horizon [Fig. 2(a)],  $\omega(k) = 0$  not only at  $k = 0$ , but also at two other non-zero momenta

$k = \pm k^*$ , corresponding to the two ‘doubler’ modes in Fig.1(b). Below, we will refer to  $\omega$  with  $|\omega| \ll 2\pi/\Delta t$  as the ‘energy’ of wave packets.

Hawking radiation emerges upon quenching the ground state of  $\hat{H}_0$  with  $U(\Delta t)$ . To measure the Hawking radiation we define the wave packet creation operators  $W_{x_0,\omega}^\dagger$ , where  $x_0$  is the location of the wave packet in real-space, and  $\omega$  its energy. Importantly, the wave packets  $W_{x_0,\omega}^\dagger$  only contain momenta near  $k = 0$  such that they are right-moving on the outside of the horizon. The time-dependent occupation number of the wave packets is given by

$$N_{x_0,\omega}(t) = \langle \psi_0(t) | W_{x_0,\omega}^\dagger W_{x_0,\omega} | \psi_0(t) \rangle, \quad (2)$$

with  $t = n\Delta t$ ,  $|\psi_0(n\Delta t)\rangle = U^n(\Delta t)|\psi_0\rangle$ , and  $|\psi_0\rangle$  is the ground state of  $\hat{H}_0$ . The initial wave packet occupation number  $N_{x_0,\omega}(0)$  for  $x_0 \gg x_b$  and  $x_0 \ll x_w$  is a step function  $\Theta(-\omega)$ , smeared over the width of the wave packet in energy space. In full agreement with the QFT case, our lattice simulations show that the quench produces outgoing particles near the horizon, with velocity  $v_{out} = v(x_0) - v_{Fl}$  (considering  $v(x)$  to be approximately constant away from the horizon). In particular, we find that after a time  $t^* \sim |x_0 - x_b|/v_{out}$  the wave-packet occupation number changes to a Fermi-Dirac distribution:

$$N_{x_0,\omega}(t \gtrsim t^*) = \frac{1}{e^{\omega/k_B T_H} + 1} := f(\omega), \quad (3)$$

with Hawking temperature  $T_H = \kappa/2\pi k_B$ , with  $\kappa = \partial_x v(x)|_{x=x_b}$  the ‘surface gravity’ of the horizon. In Fig. 3(a), we show the numerically obtained Fermi-Dirac distribution for the wave packets using  $\kappa\Delta t = 0.1$  (see [28] for the details of our numerical simulations). At larger times  $t \gtrsim t^* + |x_w - x_b|/v_{out}$ , the presence of the white hole horizon starts to affect the wave packet occupation number, and deviations from the Fermi-Dirac distribution set in.

We also calculated the occupation number of wave packets on the inside of the horizon, which we now find to go from an initial smeared out step-function  $\Theta(+\omega)$  to a Fermi-Dirac distribution with negative temperature  $-T_H$ , at times  $t \gtrsim t^* \sim |x_0 - x_b|/v_{in}$ , with  $v_{in} = v_{Fl} - v(x_0)$ . In Fig. 3(b), we plot  $|C_{max}^\omega(t_f)| = \max_j |C_{j_b - j_{in}, j_b + j}^\omega(t_f)|$ , where  $j_b = \lfloor x_b/a \rfloor$  and  $C_{ij}^\omega(t) = \langle \psi_0(t) | W_{i,\omega}^\dagger W_{j,\omega} | \psi_0(t) \rangle$  measures correlations between wave packets with equal energies at different locations. We find that the maximal wave packet correlation across the horizon occurs for  $j = j_{in}(v_{out}/v_{in})$ , and can almost perfectly be fitted with  $|C_{max}^\omega(t_f)| = \sqrt{f(\omega)f(-\omega)}$ . In Fig. 3(c), we plot the entanglement entropy of the spatial interval  $[j_b - 100, j_b]$ . It shows a linear increase of entanglement across the horizon.

Our numerical results can be understood via the following physical picture. On the outside of the black hole

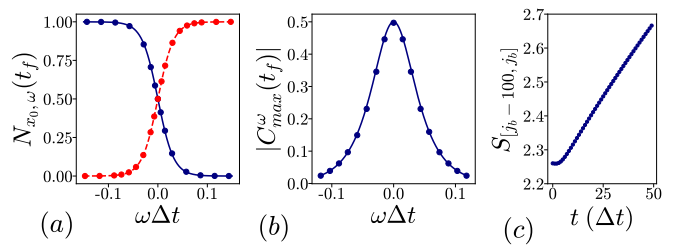


FIG. 3. Numerical results obtained using  $N = 3000$ ,  $j_b = 500$ ,  $j_w = 2500$  and  $\kappa\Delta t = 0.1$  (for more details, see supplementary material [28]). (a) wave packet occupation numbers at time  $t_f$  and position  $x_0$ . Blue points correspond to  $x_0/a = j_b + 700$  and  $t_f = 1000\Delta t$ . The blue full line is  $f(\omega)$ . Red points correspond to  $x_0/a = j_b - 450$  and  $t_f = 1200\Delta t$ . The red dashed line is  $f(-\omega)$ . (b) Maximal wave packet correlation  $|C_{max}^\omega(t_f)| = \max_j |C_{j_b - j_{in}, j_b + j}^\omega(t_f)|$  across the horizon with  $j_{in} = 450$  and  $t_f = 1000\Delta t$ . The full blue line is  $\sqrt{f(\omega)f(-\omega)}$ . (c) Entanglement entropy  $S_{[j_b - 100, j_b]}$  of the spatial interval  $[j_b - 100, j_b]$  as a function of time.

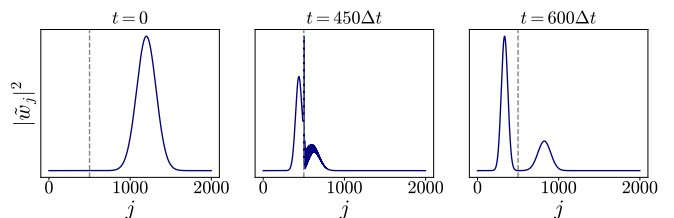


FIG. 4. Time evolution of the wave packet  $\tilde{W}_{x_0,\omega}^\dagger = \sum_j \tilde{w}_j c_j^\dagger$  made from momenta near  $-k^*$ , with  $x_0/a = j_b + 700$  and  $\omega\Delta t = 0.014$ . The dashed line is the black hole horizon, and  $\kappa\Delta t = 0.1$  was used.

horizon, the wave packets  $\tilde{W}_{x_0,\omega}^\dagger$  constructed from momenta near  $-k^*$  are occupied in the Minkowski ground state and are moving to the left, i.e. towards the horizon. In Fig. 4 we show the time-evolution of such a wave packet. We see that part of it is transmitted through the horizon, and part of it is reflected back. The reflected part corresponds to the wave packets  $W_{x_0,\omega}^\dagger$  whose occupation number is being measured in Eq. (2). From our numerics, we find that the left-moving wave packets  $\tilde{W}_{x_0,\omega}^\dagger$  are transmitted through the horizon with probability  $f(-\omega)$ , and are reflected back with probability  $f(\omega)$ . After scattering, the wave packet states thus add a contribution  $S = -f(\omega) \ln f(\omega) - f(-\omega) \ln f(-\omega)$  to the entanglement entropy across the horizon. This gives rise to a linear growth of the entanglement entropy, in accordance with the general picture for entanglement growth during quench dynamics put forward by Calabrese and Cardy [30]. To summarize, we find that Hawking radiation is the result of electrons deep inside the Fermi sea of the Minkowski ground state scattering off the horizon. As such, this realizes a fermionic lattice version of the subluminal scenario of [18, 19]. Notice also that the scattered single-particle states (right panel in Fig. 4) can

be interpreted as particle/hole Hawking-pairs, if we consider them as excitations on top of the initial Minkowski-state  $|\psi_0\rangle$ . For example, for  $\omega > 0$  we can write  $|\psi_0(t)\rangle \sim \left(\sqrt{f(-\omega)}W_{x_{in},\omega}^\dagger + \sqrt{f(\omega)}W_{x_{out},\omega}^\dagger\right)|0\rangle \sim (1 + e^{-\pi\omega/\kappa}W_{x_{out},\omega}^\dagger W_{x_{in},\omega})W_{x_{in},\omega}^\dagger|0\rangle$ .

As a final comment, let us note that the translation operator  $\hat{T}_L$  cannot be written as the exponential of a local Hamiltonian [12, 31]. This puts our model outside the well-studied class of 1D dynamics models consisting of finite-depth unitary circuits. However, our model can be realized on the edge of a 2D finite-depth quantum circuit [32–34], or by having a moving horizon and working in the co-moving frame, as in [11, 13]. This latter approach was also considered in the bosonic lattice model of Corley and Jacobson [35], see [28] for more details on the relation with our Floquet model.

*Local hamiltonian quench dynamics* – In our second approach we quench the ground state of the Minkowski Hamiltonian  $\hat{H}_0$  with the following local Hamiltonian:

$$\hat{H} = \frac{1}{2} \sum_{j=1}^N it_j c_{j+1}^\dagger c_j + \mu c_{j+1}^\dagger c_j - \mu c_j^\dagger c_j + h.c. \quad (4)$$

In the local model with periodic boundary conditions, the site-dependent hopping term  $t_j = t(ja)$  interpolates smoothly (on the lattice scale) between a constant value  $-t < 0$  in the region  $j \lesssim j_b$  and  $j \gtrsim j_w$ , which represents the analogue of the region inside the black hole, to a constant value  $t > 0$  in the region  $j_b \lesssim j \lesssim j_w$  representing the analogue of flat space outside the black hole. The specific  $t(x)$  profile that we have used in our numerics is shown in figure (5) (c). In Fig. 5 (a-b) we show the dispersion relation for the quench Hamiltonian using  $t_j = t$ , representing the outside region, and  $t_j = -t$ , representing the inside region. Note that there is a gapless mode at  $k = 0$  which is right-moving on the outside, and left-moving on the inside. As we are working with a strictly local model, there is now also an additional gapless right-moving mode in the inside region at  $k = k_{in}^* < 0$  (which is occupied in the Minkowski ground state), and an additional left-moving gapless mode at  $k = k_{out}^* > 0$  in the outside region (which is unoccupied in the Minkowski ground state). These additional modes correspond to the ‘doubler’ modes in Fig.1(c).

The terms in the Hamiltonian proportional to  $\mu$  generate a dispersion  $-\mu a^2 k^2/2$  at small  $k$ , so they do not contribute to the velocity of the zero momentum mode. Nevertheless, these terms are crucial because without them, the inside ( $t_j < 0$ ) and outside ( $t_j > 0$ ) regions are only weakly coupled. We find that for the Hawking effect to occur, the value of  $\mu$  should be larger than the surface gravity  $\kappa = a\partial_x t(x)|_{x=x_b} > 0$ . The precise value of  $\mu$  does not matter, and we will take  $\mu = 0.5t$ . We note that our Hamiltonian differs from previously studied lattice models, obtained by discretizing a Dirac fermion in a black

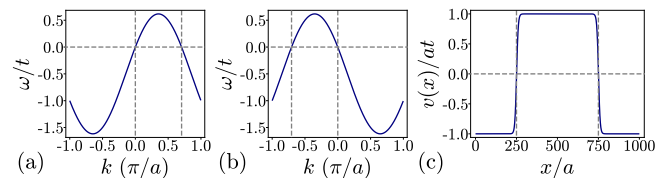


FIG. 5. (a)-(b) Dispersion relation of the local quench Hamiltonian, far away from the horizon for  $\mu = 0.5t$ . In (a),  $t_j = t$ , corresponding to the outside region. In (b),  $t_j = -t$ , corresponding to the inside region. The vertical lines show the gapless  $k = 0$  mode and doubler modes:  $k = k_{out}^*$  and  $k = k_{in}^*$ . (c) The spatially-varying velocity profile  $v(x) = at(x)$  (Eq. (64) in [28] with  $L/a = 1000$  and  $\hat{\kappa} = 0.1$ ). The locations of the two boundaries between the inside and outside regions at  $x_b = 250a$  and  $x_w = 750a$  are indicated with dashed lines.

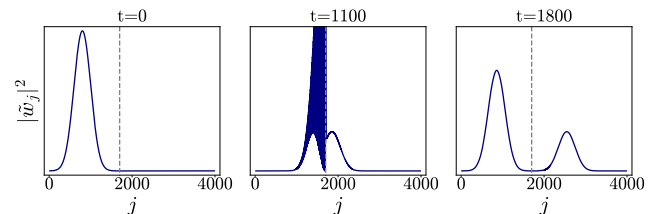


FIG. 6. Time evolution of a right-moving wave packet  $\tilde{W}_{x_0,\omega}^\dagger = \sum_j \tilde{w}_j c_j^\dagger$  starting in the inside region at  $x_0/a = j_b - 900$  with  $\omega = 0.0157t$  ( $\mu = 0.5t$ ,  $\kappa = 0.1t$ ). The dashed line shows the boundary between inside and outside regions.

hole spacetime [25–27], exactly by the terms proportional to  $\mu$ . Also note that the third term in (4) does not contribute to the dynamics (on particle-number eigenstates).

To measure the Hawking radiation in our local model we follow the same procedure as in the Floquet case: we quench the groundstate of  $\hat{H}_0$  with  $U(t) = e^{-it\hat{H}}$ , and detect the Hawking particles by measuring the wave packet occupation number as in Eq. (2). The occupation number distribution obtained in this way is identical to the Floquet result in Fig. 3 (a), and thus again shows excellent agreement with the thermal Hawking distribution (see Fig. 10 in [28]). But different from the Floquet model, the Hawking pairs now arise from the filled Fermi sea of right-moving modes near  $k = k_{in}^*$  on the inside, thereby representing a fermionic realization of the superluminal scenario of [18, 19]. In Fig. 6, we show the time evolution of such a right-moving wave packet that starts out in the inside region at  $t = 0$ . For a wave packet of energy  $\omega$ , we find that the transmission and reflection coefficients are respectively  $f(\omega)$  and  $f(-\omega)$ , which again explains both the thermal nature and the correlations of the Hawking pairs.

Instead of investigating the time-evolution of wave packets, the same results can also be obtained by constructing stationary scattering states for the Hamiltonian in Eq. (4). The Hawking temperature is contained entirely in these stationary scattering states, and the only

information needed about the Minkowski ground state is which part of these states is occupied at  $t = 0$ . We give a detailed calculation based on these scattering states in [28].

*Conclusions* – We have presented two elementary free fermion lattice models which display the Hawking effect in quench dynamics: one Floquet model with a causal horizon, and one local Hamiltonian model without a causal horizon. We find that both these models reproduce the thermal Hawking distribution found in continuum calculations. The main feature of the free fermion models is that they allow for a straightforward identification of the origin of the Hawking particles. These results now pave the way for exploring the Hawking effect in other quantum many-body systems, such as for example interacting spin chains (both analytically in integrable models, and numerically using e.g. matrix product state simulations), 2D materials with tilted Dirac cones [36–38], and cold-atom or trapped ion experiments.

*Acknowledgments* – We thank Elliot Blommaert for an initial collaboration on the project and acknowledge inspiring discussions with Gertjan Roose and Thomas Mertens. D.M. was supported by the Horizon 2020 ERC Grant No. 715861 (ERQUAF). N.B. was supported by a postdoctoral research fellowship of the Flanders Research Foundation (FWO).

- 
- [1] S. W. Hawking, Black hole explosions?, *Nature* **248**, 30 (1974).
- [2] S. W. Hawking, Particle creation by black holes, *Communications in Mathematical Physics* **43**, 199 (1975).
- [3] N. Birrell and P. Davies, *Quantum Fields in Curved Space*, Cambridge Monographs on Mathematical Physics (Cambridge University Press, 1984).
- [4] S. Fulling, F. a, and C. Series, *Aspects of Quantum Field Theory in Curved Spacetime*, EBL-Schweitzer (Cambridge University Press, 1989).
- [5] R. Wald and J. Pfister, *Quantum Field Theory in Curved Spacetime and Black Hole Thermodynamics*, Chicago Lectures in Physics (University of Chicago Press, 1994).
- [6] W. G. Unruh, Experimental black-hole evaporation?, *Phys. Rev. Lett.* **46**, 1351 (1981).
- [7] C. Barceló, S. Liberati, and M. Visser, Analogue Gravity, *Living Reviews in Relativity* **8**, 12 (2005), arXiv:gr-qc/0505065 [gr-qc].
- [8] G. W. Gibbons, Some links between general relativity and other parts of physics, in *General Relativity, Cosmology and Astrophysics: Perspectives 100 years after Einstein's stay in Prague*, edited by J. Bičák and T. Ledvinka (Springer International Publishing, Cham, 2014) pp. 91–110.
- [9] S. Weinfurter, E. W. Tedford, M. C. J. Penrice, W. G. Unruh, and G. A. Lawrence, Measurement of stimulated hawking emission in an analogue system, *Phys. Rev. Lett.* **106**, 021302 (2011).
- [10] T. A. Jacobson and G. E. Volovik, Event horizons and ergoregions in  $^3\text{He}$ , *Phys. Rev. D* **58**, 064021 (1998).
- [11] B. Horstmann, B. Reznik, S. Fagnocchi, and J. I. Cirac, Hawking Radiation from an Acoustic Black Hole on an Ion Ring, *Phys. Rev. Lett.* **104**, 250403 (2010), arXiv:0904.4801 [quant-ph].
- [12] L. J. Garay, J. R. Anglin, J. I. Cirac, and P. Zoller, Sonic black holes in dilute bose-einstein condensates, *Phys. Rev. A* **63**, 023611 (2001).
- [13] J. Steinhauer, Observation of quantum hawking radiation and its entanglement in an analogue black hole, *Nature Physics* **12**, 959 (2016).
- [14] T. Jacobson, Black-hole evaporation and ultrashort distances, *Phys. Rev. D* **44**, 1731 (1991).
- [15] W. G. Unruh, Sonic analogue of black holes and the effects of high frequencies on black hole evaporation, *Phys. Rev. D* **51**, 2827 (1995).
- [16] R. Brout, S. Massar, R. Parentani, and P. Spindel, Hawking radiation without trans-planckian frequencies, *Phys. Rev. D* **52**, 4559 (1995).
- [17] T. Jacobson, On the origin of the outgoing black hole modes, *Phys. Rev. D* **53**, 7082 (1996).
- [18] S. Corley, Computing the spectrum of black hole radiation in the presence of high frequency dispersion: An analytical approach, *Phys. Rev. D* **57**, 6280 (1998).
- [19] W. G. Unruh and R. Schützhold, Universality of the hawking effect, *Phys. Rev. D* **71**, 024028 (2005).
- [20] R. Schützhold and W. G. Unruh, Origin of the particles in black hole evaporation, *Phys. Rev. D* **78**, 041504 (2008).
- [21] A. Coutant, R. Parentani, and S. Finazzi, Black hole radiation with short distance dispersion, an analytical s-matrix approach, *Phys. Rev. D* **85**, 024021 (2012).
- [22] J. Miňar and B. Grémaud, Mimicking dirac fields in curved spacetime with fermions in lattices with non-unitary tunneling amplitudes, *Journal of Physics A: Mathematical and Theoretical* **48**, 165001 (2015).
- [23] J. Rodríguez-Laguna, L. Tarruell, M. Lewenstein, and A. Celi, Synthetic Unruh effect in cold atoms, *Phys. Rev. A* **95**, 013627 (2017), arXiv:1606.09505 [cond-mat.quant-gas].
- [24] E. Blommaert, Hamiltonian simulation of free lattice fermions in curved spacetime, *Master's thesis, Ghent University* (2019).
- [25] A. G. M. Lewis and G. Vidal, Classical Simulations of Quantum Field Theory in Curved Spacetime I: Fermionic Hawking-Hartle Vacua from a Staggered Lattice Scheme, *Quantum* **4**, 351 (2020).
- [26] R.-Q. Yang, H. Liu, S. Zhu, L. Luo, and R.-G. Cai, Simulating quantum field theory in curved spacetime with quantum many-body systems, *Phys. Rev. Research* **2**, 023107 (2020).
- [27] Y.-H. Shi, R.-Q. Yang, Z. Xiang, Z.-Y. Ge, H. Li, Y.-Y. Wang, K. Huang, Y. Tian, X. Song, D. Zheng, K. Xu, R.-G. Cai, and H. Fan, On-chip black hole: Hawking radiation and curved spacetime in a superconducting quantum circuit with tunable couplers, arXiv e-prints , arXiv:2111.11092 (2021), arXiv:2111.11092 [quant-ph].
- [28] See the supplementary material to this article, which can be found at [url].
- [29] H. Nielsen and M. Ninomiya, A no-go theorem for regularizing chiral fermions, *Physics Letters B* **105**, 219 (1981).
- [30] P. Calabrese and J. Cardy, Evolution of entanglement entropy in one-dimensional systems, *Journal of Statistical Mechanics: Theory and Experiment* **2005**, P04010 (2005).

- [31] D. Gross, V. Nesme, H. Vogts, and R. F. Werner, Index theory of one dimensional quantum walks and cellular automata, *Communications in Mathematical Physics* **310**, 419 (2012).
- [32] T. Kitagawa, E. Berg, M. Rudner, and E. Demler, Topological characterization of periodically driven quantum systems, *Phys. Rev. B* **82**, 235114 (2010).
- [33] H. C. Po, L. Fidkowski, T. Morimoto, A. C. Potter, and A. Vishwanath, Chiral floquet phases of many-body localized bosons, *Phys. Rev. X* **6**, 041070 (2016).
- [34] L. Fidkowski, H. C. Po, A. C. Potter, and A. Vishwanath, Interacting invariants for floquet phases of fermions in two dimensions, *Phys. Rev. B* **99**, 085115 (2019).
- [35] S. Corley and T. Jacobson, Lattice black holes, *Phys. Rev. D* **57**, 6269 (1998).
- [36] T. Farajollahpour, Z. Faraei, and S. A. Jafari, Solid-state platform for space-time engineering: The  $8pmmn$  borophene sheet, *Phys. Rev. B* **99**, 235150 (2019).
- [37] Y. Yekta, H. Hadipour, and S. A. Jafari, How to tune the tilt of a Dirac cone by atomic manipulations?, arXiv e-prints , arXiv:2108.08183 (2021), [arXiv:2108.08183 \[cond-mat.mtrl-sci\]](#).
- [38] A. Motavassal and S. A. Jafari, Circuit realization of tilted Dirac cone: A platform for fabrication of curved spacetime geometry on a chip, arXiv e-prints , arXiv:2110.01906 (2021), [arXiv:2110.01906 \[cond-mat.str-el\]](#).
- [39] T. Damour and R. Ruffini, Black-hole evaporation in the klein-sauter-heisenberg-euler formalism, *Phys. Rev. D* **14**, 332 (1976).
- [40] K. Srinivasan and T. Padmanabhan, Particle production and complex path analysis, *Phys. Rev. D* **60**, 024007 (1999).
- [41] M. K. Parikh and F. Wilczek, Hawking radiation as tunneling, *Phys. Rev. Lett.* **85**, 5042 (2000).
- [42] W. G. Unruh, Notes on black-hole evaporation, *Phys. Rev. D* **14**, 870 (1976).

## Supplementary material

### A. Derivation of Hawking radiation in the continuum

In this appendix we review the derivation of Hawking radiation for a continuum Dirac fermion in one spatial dimension. We start by first defining the ‘‘Minkowski’’ Hamiltonian, which is given by (working in units  $\hbar=1$ )

$$\hat{H}_0 = \int dx \psi^\dagger(x) (-iv\partial_x) \psi(x). \quad (5)$$

Here,  $v$  is a velocity, and  $\psi^\dagger(x)$ ,  $\psi(x)$  are creation and annihilation operators satisfying the canonical fermionic anti-commutation relations:

$$\{\psi^\dagger(x), \psi(x')\} = \delta(x - x') \quad (6)$$

$$\{\psi^\dagger(x), \psi^\dagger(x')\} = \{\psi(x), \psi(x')\} = 0. \quad (7)$$

The Minkowski Hamiltonian  $\hat{H}_0$  describes the right-moving part of a massless Dirac fermion in one spatial dimension. We ignore the left-moving part of the Dirac fermion because it does not play any role in the Hawking effect. The ground state  $|\psi_0\rangle$  of  $H_0$  is obtained by occupying all plane wave state with negative energy  $E(k) = vk$ , and thus satisfies

$$\langle \psi_0 | \psi_k^\dagger \psi_{k'} | \psi_0 \rangle = \Theta(-k) \delta(k - k'), \quad (8)$$

with  $\psi_k^\dagger = (2\pi)^{-1/2} \int dx e^{ikx} \psi^\dagger(x)$ .

Besides the Minkowski Hamiltonian, we also need a horizon Hamiltonian  $\hat{H}_h$ , which is given by

$$\hat{H}_h = \int dx \psi^\dagger(x) \left( -iv(x)\partial_x - \frac{i}{2}\partial_x v(x) \right) \psi(x) := \int dx \psi^\dagger(x) \hat{h}_h \psi(x). \quad (9)$$

In the horizon Hamiltonian, the velocity  $v(x)$  is a continuous function of  $x$  which satisfies  $v(x) > 0$  for  $x > 0$ , and  $v(x) < 0$  for  $x < 0$ . The horizon is located at  $x = 0$ , where  $v(0) = 0$ . The region  $x > 0$  is called the ‘outside’

region of the horizon, and  $x < 0$  is the ‘inside’ region. In the presence of an additional mode which is everywhere left moving (recall that we ignoring this mode here), it is possible to move both left and right for  $x > 0$ , whereas for  $x < 0$  one is forced to move to the left which means that it is impossible to cross the horizon (one is trapped behind the horizon). The term  $-i\partial_x v(x)\psi^\dagger(x)\psi(x)/2$  is necessary to ensure that the horizon Hamiltonian is hermitian.

In this appendix we will be interested in two different velocity profiles:

$$v(x) = \kappa x, \quad [\text{Unruh case}] \quad (10)$$

$$v(x) = v \tanh(x\kappa/v). \quad [\text{Hawking case}] \quad (11)$$

Here,  $\kappa$ , which has dimensions of inverse time (or energy since  $\hbar = 1$ ), is the ‘surface gravity’. The first velocity profile  $v(x) = \kappa x$  corresponds to a Rindler observer, which has a constant acceleration. This case was analysed by Unruh, and we will therefore call this the Unruh case. The second velocity profile  $v(x) = v \tanh(\kappa x/v)$  goes to  $\pm v$  as  $x \rightarrow \pm\infty$ . So in this case, the horizon hamiltonian is a ‘black hole’ Hamiltonian which matches the Minkowski hamiltonian far away on the right hand side of the horizon (this is the ‘outside’ of the black hole). The black hole case was analysed by Hawking, and so we refer to it as the Hawking case. Below, we discuss the Unruh and Hawking cases separately.

### 1. Unruh/Rindler case

We start by finding the eigenstates of the single-particle Hamiltonian  $\hat{h}_h$  in Eq. (9) with the Unruh velocity profile  $v(x) = \kappa x$ . For this we use the ansatz  $\varphi(x) = \exp(iS(x))$ . This state is an eigenstate with energy  $\omega$  if

$$\omega = v(x)\partial_x S(x) - \frac{i}{2}\partial_x v(x) \quad (12)$$

The solutions to this equation are

$$S^\pm(x) = \lim_{\epsilon \rightarrow 0^\pm} \int^x dx' \frac{\omega + i\partial_{x'} v(x')/2}{v(x') + i\epsilon} \quad (13)$$

$$= \mathcal{P} \int^x dx' \frac{\omega}{v(x')} \mp i \frac{\pi\omega}{\kappa} \Theta(x) \quad (14)$$

$$+ \frac{i}{2} \mathcal{P} \int^x dx' \partial_{x'} \ln(v(x')) \pm \frac{\pi}{2} \Theta(x) \quad (15)$$

$$= \mathcal{P} \int^x dx' \frac{\omega}{v(x')} \mp i \frac{\pi\omega}{\kappa} \Theta(x) + \frac{i}{2} \ln(|v(x)|) \pm \frac{\pi}{2} \Theta(x), \quad (16)$$

where  $\mathcal{P}$  denotes the Cauchy principal value and  $\Theta(x)$  is the Heaviside step function. A similar  $i\epsilon$  prescription was also previously used in Refs. [39–41]. Plugging these solutions for  $S(x)$  back in the ansatz  $\varphi(x) = \exp(iS(x))$ , we find two solutions for the Rindler eigenstates with energy  $\omega$ :

$$\varphi_\omega^{R+}(x) = \Theta(-x) \frac{1}{\sqrt{-\kappa x}} e^{i\omega \ln(-\kappa x)/\kappa} + \Theta(x) \frac{e^{i\pi/2} e^{\pi\omega/\kappa}}{\sqrt{\kappa x}} e^{i\omega \ln(\kappa x)/\kappa} \quad (17)$$

$$\varphi_\omega^{R-}(x) = \Theta(-x) \frac{1}{\sqrt{-\kappa x}} e^{i\omega \ln(-\kappa x)/\kappa} + \Theta(x) \frac{e^{-i\pi/2} e^{-\pi\omega/\kappa}}{\sqrt{\kappa x}} e^{i\omega \ln(\kappa x)/\kappa} \quad (18)$$

Using

$$\int_0^\infty dx \frac{1}{\kappa x} e^{i(\omega-\omega') \ln(\kappa x)/\kappa} = \int_{-\infty}^\infty d(\ln(\kappa x)/\kappa) e^{i(\omega-\omega') \ln(\kappa x)/\kappa} \quad (19)$$

$$= 2\pi\delta(\omega - \omega') \quad (20)$$

we see that the Rindler wavefunctions in Eqs. (17)-(18) satisfy

$$\int dx [\varphi_\omega^{Rs}(x)]^* \varphi_{\omega'}^{Rs'}(x) = 2\pi(1 + e^{s2\pi\omega/\kappa})\delta_{s,s'}\delta(\omega - \omega'), \quad (21)$$

where  $s, s' = \pm$ .

A crucial observation is that the Rindler eigenfunctions can be written as

$$\varphi_\omega^{R+}(x) = \int_0^\infty dk e^{ikx} \tilde{\varphi}_\omega^{R+}(k), \quad (22)$$

$$\varphi_\omega^{R-}(x) = \int_0^\infty dk e^{-ikx} \tilde{\varphi}_\omega^{R-}(k). \quad (23)$$

As pointed out by Unruh [42], this follows from the fact that any function which only has positive (negative) Fourier modes is analytic in the upper (lower) half of the complex plane. The branch cuts of the logarithm and the square root in  $\varphi_\omega^{R+}(x)$  ( $\varphi_\omega^{R-}(x)$ ) both lie in the lower (upper) half-plane, which means that  $\varphi_\omega^{R+}(x)$  ( $\varphi_\omega^{R-}(x)$ ) is analytic in the upper (lower) half plane. From this observation we learn that  $\varphi_\omega^{R+}(x)$  is made entirely from states which are unoccupied in the Minkowski vacuum, whereas  $\varphi_\omega^{R-}(x)$  made entirely from states which are occupied in the Minkowski vacuum. Because the set of occupied (unoccupied) plane wave states in the Minkowski vacuum and the Rindler wavefunctions  $\varphi_\omega^{R-}(x)$  ( $\varphi_\omega^{R+}(x)$ ) are related via an invertible linear transformation, we conclude that

$$\langle \psi_0 | \psi_{R,s}^\dagger(\omega) \psi_{R,s'}(\omega') | \psi_0 \rangle = \begin{cases} \delta(\omega - \omega') & \text{if } s = s' = - \\ 0 & \text{otherwise} \end{cases}, \quad (24)$$

where

$$\psi_{R-}^\dagger(\omega) = \frac{1}{\sqrt{1 + e^{-2\pi\omega/\kappa}}} \frac{1}{\sqrt{2\pi}} \int dx \varphi_\omega^{R-}(x) \psi^\dagger(x), \quad (25)$$

$$\psi_{R+}^\dagger(\omega) = \frac{1}{\sqrt{1 + e^{2\pi\omega/\kappa}}} \frac{1}{\sqrt{2\pi}} \int dx \varphi_\omega^{R+}(x) \psi^\dagger(x), \quad (26)$$

are fermion creation operators satisfying

$$\{\psi_{Rs}^\dagger(\omega), \psi_{Rs'}(\omega')\} = \delta_{s,s'} \delta(\omega - \omega') \quad (27)$$

$$\{\psi_{Rs}^\dagger(\omega), \psi_{Rs'}^\dagger(\omega')\} = \{\psi_{Rs}(\omega), \psi_{Rs'}(\omega')\} = 0. \quad (28)$$

Finally, we define the ‘single-sided’ eigenstate creation operators as follows:

$$\psi_{R,out}^\dagger(\omega) = \frac{1}{\sqrt{2\pi}} \int_0^\infty dx \frac{1}{\sqrt{\kappa x}} e^{i\omega \ln(\kappa x)/\kappa} \psi^\dagger(x) \quad (29)$$

$$\psi_{R,in}^\dagger(\omega) = \frac{1}{\sqrt{2\pi}} \int_{-\infty}^0 dx \frac{1}{\sqrt{-\kappa x}} e^{i\omega \ln(-\kappa x)/\kappa} \psi^\dagger(x). \quad (30)$$

These creation operators again satisfy the canonical fermionic anti-commutation relations:

$$\{\psi_{R,l}^\dagger(\omega), \psi_{R,l'}(\omega')\} = \delta_{l,l'} \delta(\omega - \omega'), \quad (31)$$

$$\{\psi_{R,l}^\dagger(\omega), \psi_{R,l'}^\dagger(\omega')\} = \{\psi_{R,l}(\omega), \psi_{R,l'}(\omega')\} = 0, \quad (32)$$

where  $l, l' = in/out$ . From their definition, it is clear that the single-sided eigenmodes can be obtained as linear combinations of the degenerate wavefunctions  $\varphi_\omega^{R+}(x)$  and  $\varphi_\omega^{R-}(x)$ . In particular, it holds that

$$\begin{aligned}
\psi_{R,in}^\dagger(\omega) &= \frac{1}{\sqrt{1+e^{2\pi\omega/\kappa}}} \psi_{R,+}^\dagger(\omega) + \frac{1}{\sqrt{1+e^{-2\pi\omega/\kappa}}} \psi_{R,-}^\dagger(\omega), \\
\psi_{R,out}^\dagger(\omega) &= -i \frac{e^{\pi\omega/\kappa}}{\sqrt{1+e^{2\pi\omega/\kappa}}} \psi_{R,+}^\dagger(\omega) + i \frac{e^{-\pi\omega/\kappa}}{\sqrt{1+e^{-2\pi\omega/\kappa}}} \psi_{R,-}^\dagger(\omega)
\end{aligned} \tag{33}$$

From these relations, and Eq. (24), we find that

$$\langle \psi_0 | \psi_{R,out}^\dagger(\omega) \psi_{R,out}(\omega') | \psi_0 \rangle = \frac{1}{e^{2\pi\omega/\kappa} + 1} \delta(\omega - \omega') := f(\omega) \delta(\omega - \omega') \tag{34}$$

This is the famous Unruh result [42]: after tracing out the region behind the horizon of an accelerating Rindler observer, the density matrix of the outer region is a thermal state with temperature  $T = \kappa/2\pi k_B$  of the Rindler modes which only have support on the outside of the horizon. The Bogoliubov transformations (33) can also be used to compute the occupation numbers for the inside (left-moving) modes and the correlation between the inside and outside modes:

$$\langle \psi_0 | \psi_{R,in}^\dagger(\omega) \psi_{R,in}(\omega') | \psi_0 \rangle = \frac{1}{e^{-2\pi\omega/\kappa} + 1} \delta(\omega - \omega') = f(-\omega) \delta(\omega - \omega'), \tag{35}$$

$$\langle \psi_0 | \psi_{R,in}^\dagger(\omega) \psi_{R,out}(\omega') | \psi_0 \rangle = -i \frac{e^{-\pi\omega/\kappa}}{e^{-2\pi\omega/\kappa} + 1} \delta(\omega - \omega') = -i \sqrt{f(\omega) f(-\omega)} \delta(\omega - \omega'), \tag{36}$$

Note that we have also found that the Minkowski ground state is an eigenstate of the Rindler Hamiltonian:  $H_h = \int d\omega \omega \left( \psi_{R+}^\dagger(\omega) \psi_{R+}(\omega) + \psi_{R-}^\dagger(\omega) \psi_{R-}(\omega) \right)$ . So if we were to quench the Minkowski ground state with the Rindler Hamiltonian, this would not generate any non-trivial dynamics.

## 2. Hawking/black hole case

Let us now consider the horizon Hamiltonian in Eq. (9) with the black hole velocity profile  $v(x) = v \tanh(\kappa x/v)$ . We want to show that Hawking radiation emerges upon quenching the Minkowski ground state with this Hamiltonian.

For large positive  $x$ , the black hole velocity profile approaches a constant velocity  $v$ . So far outside the black hole, the Minkowski ground state looks like the ground state of the black hole Hamiltonian, and no non-trivial dynamics will originate from this region. For large negative  $x$ , the black hole velocity profile approaches the constant velocity  $-v$ . In this region, the Minkowski ground state is again an eigenstate of the black hole Hamiltonian, but it is no longer the ground state. Instead,  $|\psi_0\rangle$  locally looks like the highest energy eigenstate of  $\hat{H}_h$ . Nevertheless, the region far away on the inside of the black hole will again not generate any non-trivial dynamics. Close to the horizon, we can approximate the black hole velocity profile as  $v(x) \sim \kappa x$ , which is exactly the Rindler velocity profile. From our previous analysis of the Unruh/Rindler case, we conclude that close to the horizon, the Minkowski ground state looks like a finite-temperature state with temperature  $T = \kappa/2\pi k_B$  for the black hole Hamiltonian. Again we expect that the region close to the horizon where  $v(x) \sim \kappa x$  will not generate any non-trivial dynamics, because in the previous section we found that the Minkowski ground state is an eigenstate of the Rindler Hamiltonian.

The previous discussion suggests the following physical picture: for the black hole Hamiltonian, the Minkowski ground state looks like a state with a temperature profile  $T(x) \propto \partial_x v(x)$ . Far on the outside, the temperature is  $T(x \gg v\kappa^{-1}) \sim 0^+$  and the Minkowski ground state is effectively the black hole ground state. Far on the inside,  $T(x \ll -v\kappa^{-1}) \sim 0^-$ , and the Minkowski ground state looks like the highest energy state. Close to the horizon on the outside,  $T(0 < x \ll v\kappa^{-1}) = \kappa/2\pi k_B$ . And close to the horizon on the inside,  $T(0 > x \gg -v\kappa^{-1}) \sim -\kappa/2\pi k_B$  (see Eq.(35)). Gradients in the temperature occur in regions where the velocity has a non-zero curvature:  $\partial_x T(x) \propto \partial_x^2 v(x)$ . The Hawking effect corresponds to the emission of particles from the ‘hot’ to the ‘cold’ regions in the Minkowski ground state under a quench with the black hole Hamiltonian. These particles originate from the regions where  $\partial_x^2 v(x) \neq 0$ , which is roughly at a distance  $v\kappa^{-1}$  away from the horizon.

To make this physical picture more concrete, we will first calculate the occupation number of wave packets on the outside of the horizon. We define the wave packet creation operator as:

$$W_{x_0, k_0}^\dagger = \int dx w_{x_0, k_0}(x) \psi^\dagger(x), \quad (37)$$

with

$$w_{x_0, k_0}(x) = \frac{1}{(2\pi\sigma^2)^{1/4}} \int_{-\infty}^{+\infty} dk e^{-\frac{(k-k_0)^2}{4\sigma^2}} \frac{1}{\sqrt{2\pi}} e^{ik(x-x_0)}, \quad (38)$$

a Gaussian wave-packet, with the momentum centered around  $k_0$  and the position centered around  $x_0$ . The occupation number  $N_{x_0, k_0}(t)$  of this packet can be found as:

$$\begin{aligned} N_{x_0, k_0}(t) &= \langle \psi_0(t) | W_{x_0, k_0}^\dagger W_{x_0, k_0} | \psi_0(t) \rangle \\ &= \langle \psi_0 | e^{itH_h} W_{x_0, k_0}^\dagger W_{x_0, k_0} e^{-itH_h} | \psi_0 \rangle \\ &= \langle \psi_0 | W_{x_0, k_0}^\dagger(-t) W_{x_0, k_0}(-t) | \psi_0 \rangle, \end{aligned} \quad (39)$$

with:

$$\begin{aligned} W_{x_0, k_0}^\dagger(-t) &:= \int dx w_{x_0, k_0} e^{itH_h} \psi^\dagger(x) e^{-itH_h} \\ &= \int dx w_{x_0, k_0}(x) e^{+it h_h^*} \psi^\dagger(x) \\ &= \int dx (e^{+it h_h} w_{x_0, k_0}(x)) \psi^\dagger(x) \\ &= \int dx w_{x_0, k_0}(x, -t) \psi^\dagger(x). \end{aligned} \quad (40)$$

where in the last line the wave-packet  $w_{x_0, k_0}(x, -t) = e^{+it h_h} w_{x_0, k_0}(x)$  is propagated back(!) in time with the single-particle Hamiltonian  $h_h$  (cfr. Eq. (9)). To obtain  $w_{x_0, k_0}(x, -t)$  it is useful to look at the expressions for the eigen out-modes, which from a generalisation of the Unruh/Rindler case, are readily found as:

$$\varphi_\omega^{out}(x) = \Theta(x) \frac{1}{\sqrt{2\pi v(x)}} e^{i\omega \int^x dx' \frac{1}{v(x')}} = \Theta(x) \frac{1}{\sqrt{2\pi v \tanh(\kappa x/v)}} e^{i\omega \ln(\sinh(\kappa x/v))/\kappa}. \quad (41)$$

Far away from the horizon,  $x \gg v/\kappa$ , we effectively have Minkowski space-time and  $\varphi_\omega^{out}$  reduces to a plane wave; on the other hand, close to the horizon,  $x \ll v/\kappa$ , we have effectively the Rindler case and  $\varphi_\omega^{out}$  reduces to  $\varphi_\omega^{R, out}$ , explicitly:

$$\varphi_\omega^{out}(x) \stackrel{x \gg v/\kappa}{=} \frac{1}{\sqrt{2\pi v}} e^{i\frac{\omega}{v}(x - \frac{v}{\kappa} \ln(2))} \quad \varphi_\omega^{out}(x) \stackrel{x \ll v/\kappa}{=} \frac{1}{\sqrt{2\pi \kappa x}} e^{i\omega \ln(\kappa x/v)/\kappa} = e^{-i\omega \ln(v)/\kappa} \varphi_\omega^{R, out}(x). \quad (42)$$

Taking the initial wave-packet  $w_{x_0, k_0}$  (Eq. 38) far from the horizon,  $x_0 \gg v/\kappa$ , we can now effectively write:

$$w_{x_0, k_0}(x) = \frac{1}{(2\pi\sigma^2 v^2)^{1/4}} \int_{-\infty}^{+\infty} d\omega e^{-\frac{(\omega - vk_0)^2}{4\sigma^2 v^2}} e^{i\frac{\omega}{v}(\frac{v}{\kappa} \ln(2) - x_0)} \varphi_\omega^{out}(x), \quad (43)$$

which in turn allows to find the time-evolved wave-packet:

$$w_{x_0, k_0}(x, -t) = \frac{1}{(2\pi\sigma^2 v^2)^{1/4}} \int_{-\infty}^{+\infty} d\omega e^{-\frac{(\omega - vk_0)^2}{4\sigma^2 v^2}} e^{i\frac{\omega}{v}(\frac{v}{\kappa} \ln(2) - x_0 + vt)} \varphi_\omega^{out}(x), \quad (44)$$

$$= \frac{1}{\sqrt{v(x)}} \frac{1}{(2\pi\sigma^2 v^2)^{1/4}} \int_{-\infty}^{+\infty} d\omega e^{-\frac{(\omega - vk_0)^2}{4\sigma^2 v^2}} e^{i\frac{\omega}{v}(\frac{v}{\kappa} \ln(2) - x_0 + vt + y(x))}, \quad (45)$$

where on the last line we have introduced the ‘tortoise’-coordinate  $y(x) = \int^x dx' v/v(x') = v/\kappa \ln(\sinh(\kappa x/v))$ . Notice that

$$y(x) \stackrel{x \gg v/\kappa}{=} x - \frac{v}{\kappa} \ln(2) \quad y(x) \stackrel{x \ll v/\kappa}{=} \frac{v}{\kappa} \ln(\kappa x/v), \quad (46)$$

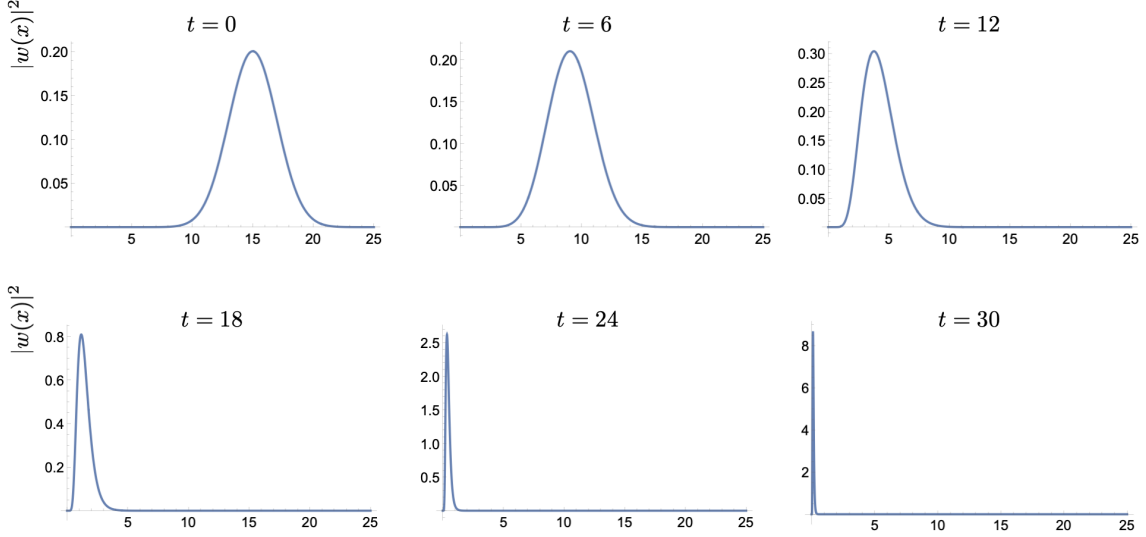


FIG. 7. Backwards-in-time evolution of the wave packet  $w_{x_0, k_0}(x, -t)$  (Eq. (44)) with  $x_0 = 15, k_0 = 5, \sigma = 0.25, v = 1$  and  $\kappa = 5$ . Notice the alteration in the wave packet behaviour upon entering the quantum atmosphere at  $x \approx v/\kappa = 5$ .

in particular we have that  $y(x) \rightarrow -\infty$  when  $x \rightarrow 0+$ . We see that up to the pre-factor  $v(x)^{-1/2}$  the wave-packet  $w_{x_0, k_0}(x, -t)$  consists of plane-waves in  $y$ -space and therefore find that the wave-packet moves with constant width  $\Delta y \sim 1/\sigma$  and constant velocity  $-v$  in  $y$ -space:  $y_c(t) = x_0 - \frac{v}{\kappa} \ln(2) - vt$ , where  $y_c(t)$  denotes the centre-position of the packet. In  $x$ -space this translates to a wave-packet propagating with constant width and constant velocity  $-v$ , as long as  $x_c(t) \gg v/\kappa$ . This behaviour changes when the wave-packet enters the ‘quantum-atmosphere’  $|x| \lesssim v/\kappa$ , around  $t = t^* \sim x_0/v - 1/\kappa$ . Inside the quantum atmosphere, the wave-packet will start to contract,  $\Delta x \sim \Delta y/y'(x_c) \sim v(x_c)/(v\sigma)$  and slow down,  $\dot{x}_c \sim \dot{y}_c/y'(x_c) = v(x_c)$ , asymptotically ( $t \rightarrow \infty$ ) ‘freezing’ on the horizon  $x = 0$ . We illustrate this behaviour in Fig. 7.

Summarising, the wave-packet evolution has essentially two regimes: for  $t \lesssim t^*$  it has only non-trivial support outside the quantum atmosphere,  $x > v/\kappa$ , while for  $t \gtrsim t^*$  it will end up lying completely inside the quantum atmosphere  $0 < x < v/\kappa$ . From (42) and (44) we see that this implies, that for  $t \lesssim t^*$  the wave-packet remains a superposition of Minkowski plane-waves, while for  $t \gtrsim t^*$  it reduces to a superposition of Rindler eigen-modes, explicitly:

$$W_{x_0, k_0}^\dagger(-t) \stackrel{t \ll t^*}{\approx} \frac{1}{(2\pi\sigma^2 v^2)^{1/4}} \int_{-\infty}^{+\infty} d\omega e^{-\frac{(\omega - vk_0)^2}{4\sigma^2 v^2}} e^{i\frac{\omega}{v}(\frac{v}{\kappa} \ln(2) - x_0 + vt)} \psi_M^\dagger(\omega) \quad (47)$$

$$W_{x_0, k_0}^\dagger(-t) \stackrel{t \gg t^*}{\approx} \frac{1}{(2\pi\sigma^2 v^2)^{1/4}} \int_{-\infty}^{+\infty} d\omega e^{-\frac{(\omega - vk_0)^2}{4\sigma^2 v^2}} e^{i\frac{\omega}{v}(\frac{v}{\kappa} \ln(2) - x_0 + vt)} \psi_{R, out}^\dagger(\omega) \quad (48)$$

Finally, evaluating  $N_{x_0, k_0}(t) = \langle \psi_0 | W_{x_0, k_0}^\dagger(-t) W_{x_0, k_0}(-t) | \psi_0 \rangle$  we find that this gives a smeared out step-function  $\Theta(-\omega)$  (with  $\omega = k_0 v$ ) at initial times  $t \ll t^*$ ; going over into the Fermi-Dirac distribution  $f(\omega)$  at later times  $t \gg t^*$  (see (34)), provided that  $v\sigma \ll k_B T_H = \frac{\kappa}{2\pi}$ . This is also precisely what we find in our lattice simulations as discussed in the main text.

In a completely similar fashion one can consider the time-evolution of a wave-packet, initially deep inside the black hole ( $x_0 \ll -v/\kappa$ ), resulting in (with now  $t^* = -x_0/v - 1/\kappa$ ):

$$W_{x_0, k_0}^\dagger(-t) \stackrel{t \ll t^*}{\approx} \frac{1}{(2\pi\sigma^2 v^2)^{1/4}} \int_{-\infty}^{+\infty} d\omega e^{-\frac{(\omega + vk_0)^2}{4\sigma^2 v^2}} e^{i\frac{\omega}{v}(\frac{v}{\kappa} \ln(2) + x_0 + vt)} \psi_M^\dagger(-\omega) \quad (49)$$

$$W_{x_0, k_0}^\dagger(-t) \stackrel{t \gg t^*}{\approx} \frac{1}{(2\pi\sigma^2 v^2)^{1/4}} \int_{-\infty}^{+\infty} d\omega e^{-\frac{(\omega + vk_0)^2}{4\sigma^2 v^2}} e^{i\frac{\omega}{v}(\frac{v}{\kappa} \ln(2) + x_0 + vt)} \psi_{R, in}^\dagger(\omega). \quad (50)$$

This then gives  $N_{x_0, k_0}(t)$  going from the smeared out step-function  $\Theta(\omega)$  (with now  $\omega = -k_0 v$ ) at  $t \ll t^*$  to  $f(-\omega)$  at times  $t \gg t^*$ , again in agreement with our lattice results. Finally, for the wave-packet correlation function (for

$t \gg -x_{in}/v - 1/\kappa, x_{out}/v - 1/\kappa$  and with  $k_{in} = -\omega_0/v, k_{out} = +\omega_0/v$ ) we get (from (36)):

$$\langle \psi_0 | W_{x_{in}, k_{in}}^\dagger(-t) W_{x_{out}, k_{out}}(-t) | \psi_0 \rangle = -\frac{i}{(2\pi\sigma^2 v^2)^{1/2}} \int_{-\infty}^{+\infty} d\omega e^{-\frac{(\omega-\omega_0)^2}{2\sigma^2 v^2}} e^{i\frac{\omega}{v}(x_{in}+x_{out})} \sqrt{f(\omega)f(-\omega)} \quad (51)$$

$$\approx -i\sqrt{f(\omega_0)f(-\omega_0)} e^{i\frac{\omega_0}{v}(x_{in}+x_{out})} e^{-\frac{\sigma^2(x_{in}+x_{out})^2}{2}}, \quad (52)$$

where on the last line we again assumed  $v\sigma \ll k_B T_H$ . This is the continuum version of our lattice results on the particle correlations (see e.g. Fig. 3(b) and the corresponding discussion in the main text).

The region inside the quantum atmosphere  $-\kappa/v \lesssim x \lesssim +\kappa/v$  is not altered during the evolution, yet it acts like an infinite reservoir for the outgoing radiation, with arbitrary short ('transPlanckian') wavelength modes, that upon leaving the horizon get redshifted to their asymptotic value (see e.g. Fig. 7). This is very different for the lattice models that we discuss in the main text, where the outgoing radiation finds its origin in a bulk reservoir of ingoing doubler modes on the outside (for the Floquet model) or in a bulk reservoir of outgoing doubler modes on the inside of the boundary (for the local model).

## B. Details of numerical simulations for the Floquet model

For our numerical calculations, we use the following explicit expression for  $t(x)$ :

$$t(x) = t \left( \frac{4}{\pi b} \arctan \left[ \frac{\cosh(\tilde{\kappa}\pi W/4)}{\cosh(\pi\tilde{\kappa}(x-L/2)/2)} \right] + \frac{b-1}{b} \right)^b, \quad (53)$$

where  $L = Na$  is the length of the system, and  $\tilde{\kappa}$  and  $b$  are free parameters. We take the overall energy scale to be  $t = (\Delta t)^{-1}$ , such that  $at(x) = a/\Delta t = v_{Fl}$  at the location of the black hole horizon  $x_b = L/2 - W/2$ , and at the location of the white hole horizon  $x_w = L/2 + W/2$ . The surface gravity is given by  $\kappa = at\tilde{\kappa} \tanh(\tilde{\kappa}\pi W/4)$ . For a sufficiently large width  $W$  of the region outside the horizon (we always take  $W$  to be a couple of hundred lattice sites), we effectively have  $\kappa = \tilde{\kappa}v_{Fl}$ .

The wave packet operators  $W_{x_0, \omega}^\dagger$  are defined as follows:

$$W_{x_0, \omega}^\dagger = \mathcal{N} \sum_{k=-\pi/a}^{\pi/a} e^{-(k-\omega/v_{out})^2/4\sigma^2} e^{-ikx_0} c_k^\dagger \quad \text{for } x_b < x_0 < x_w, \quad (54)$$

$$W_{x_0, \omega}^\dagger = \mathcal{N} \sum_{k=-\pi/a}^{\pi/a} e^{-(k+\omega/v_{in})^2/4\sigma^2} e^{-ikx_0} c_k^\dagger \quad \text{for } x_0 < x_b, \quad (55)$$

where  $\mathcal{N}$  is a normalization factor, and  $c_k^\dagger = \frac{1}{\sqrt{N}} \sum_{j=1}^N e^{ikaj} c_j^\dagger$ . As mentioned in the main text, we always take  $|\omega\Delta t| \ll 1$ . The quantities  $v_{out} = v(x \gg x_b) - v_{Fl}$  and  $v_{in} = v_{Fl} - v(x \ll x_b)$  are (the absolute values of) the velocities of the wave packets on respectively the outside and inside of the black hole horizon. The velocity profile  $v(x)$  is approximately constant for  $|x - x_b|, |x - x_w| \gg \tilde{\kappa}^{-1}$ .

We calculate the time-dependent wave packet occupation number  $N_{x_0, \omega}(n\Delta t)$  in practice by writing it as  $N_{x_0, \omega}(n\Delta t) = \langle \psi_0 | W_{x_0, \omega}^\dagger(-n\Delta t) W_{x_0, \omega}(-n\Delta t) | \psi_0 \rangle$ , where  $W_{x_0, \omega}^\dagger(-n\Delta t) = U^{-n}(\Delta t) W_{x_0, \omega}^\dagger U^n(\Delta t)$  is the wave packet operator evolved *backwards* in time; and where in analogy with the continuum case we define  $W_{x_0, \omega}^\dagger(t) := \sum_i w_i^{x_0, \omega}(t) c_i^\dagger$ , with  $w_i^{x_0, \omega}(t)$  obtained from evolving with the single-particle Schrödinger equation. In Fig. 8, we show an example of such a backwards-in-time evolved wave packet on the outside of the black hole horizon. Note that because we evolve backwards in time, the right-moving wave packet moves to the left, i.e. it moves closer to the black hole horizon. From Fig. 8 we see that during the time evolution the wave packet does not cross the horizon, but instead develops very short-wavelength oscillations and subsequently bounces back to the outside region. In Ref. [35] this was interpreted as a Bloch oscillation.

For the calculation of the wave packet occupation numbers in Fig. 3, the width of the wave packets in momentum space was  $\sigma = 2(2\pi/L)$ . For the calculation of the wave packet correlations across the horizon in Fig. 3, we used  $\sigma = 2(2\pi/L)$  for the wave packets behind the horizon, and  $\sigma = 2(2\pi/L) \times (v_{in}/v_{out})$  for the wave packets on the outside of the horizon. This relation between the widths of the wave packets is important for the maximal wave packet correlations to be given by  $\sqrt{f(\omega)f(-\omega)}$ .

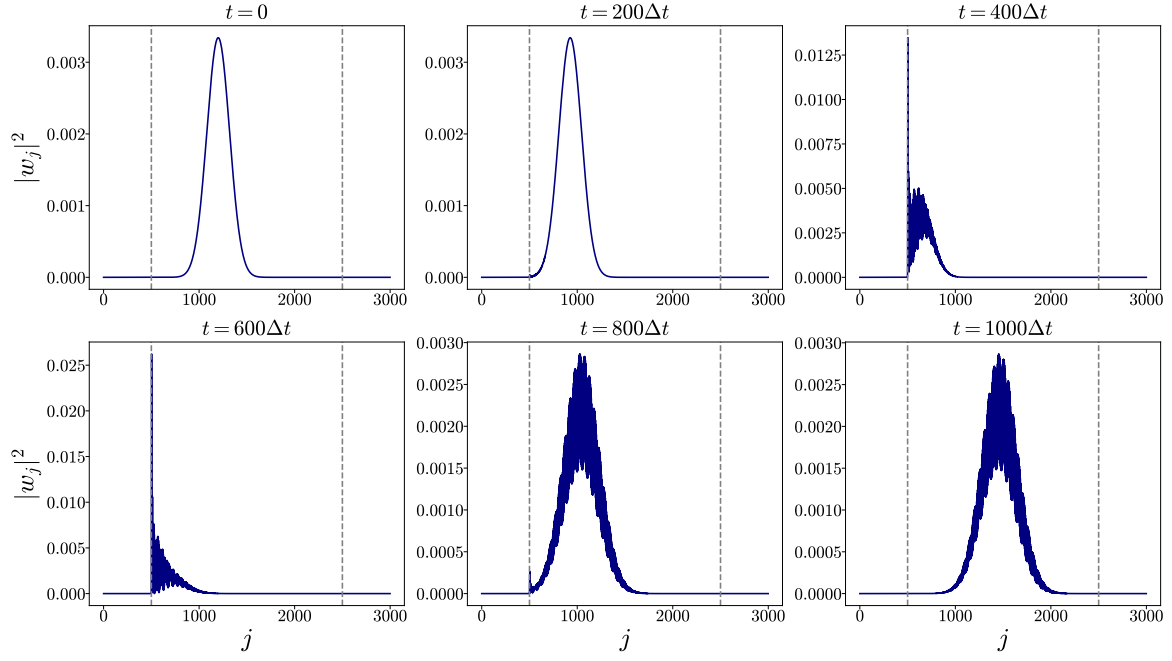


FIG. 8. Backwards-in-time evolution of the wave packet  $W_{x_0, \omega}^\dagger = \sum_j w_j c_j^\dagger$  with  $x_0 = x_b + 700a$  and  $\omega = 0.057t$ . The width of the wave packet in momentum space is  $\sigma = 2(2\pi/L)$ . The system size is  $N = 3000$ ,  $x_b = 500a$  and  $x_w = 2500a$ . The function  $t(x)$  in Eq. (53) was used with  $\tilde{\kappa}a = 0.1$  and  $b = 3$ .

The left-moving wave packet operators  $\tilde{W}_{x_0, \omega}^\dagger$  used in Fig. 4 are defined as

$$\tilde{W}_{x_0, \omega}^\dagger = \mathcal{N} \sum_{k=-\pi/a}^{\pi/a} e^{-(k+k^*+\omega/v^*)^2/4\sigma^2} e^{-ikx_0} c_k^\dagger, \quad (56)$$

where  $v^* = |\partial_k \omega(k)|_{k=-k^*}$  (with  $v = v(x \gg x_b)$ ) is the velocity of the wave packets. The width used in Fig. 4 was again  $\sigma = 2(2\pi/L)$ .

### C. Connection between the Corley-Jacobson falling lattice and static horizons in Floquet systems

In Ref. [35], Corley and Jacobson discretized a scalar field on a spatial lattice which is falling into a black hole. As a result of this choice of discretization, the location of the horizon relative to the lattice changes in time. The Corley-Jacobson falling lattice analogue of our fermion hopping model used in the main text would therefore correspond to the following time-dependent Hamiltonian:

$$\hat{H}_{CJ}(t) = \sum_{j=1}^N \frac{t_j(t) + t_{j+1}(t)}{4} (ic_{j+1}^\dagger c_j - ic_j^\dagger c_{j+1}), \quad (57)$$

where  $t_j(t) = t(ja - v_{Fl}t)$ , with  $t(x)$  the same continuous function as used in the main text. Note that it is common in the literature to denote both the hopping strength and time with the same symbol  $t$ . From the context the meaning should be clear. In the Corley-Jacobson model, the location of the horizon is moving to the right with a velocity  $v_{Fl} = a/\Delta t$ . Particles in the region to the left of the black hole horizon move slower than  $v_{Fl}$ , so they can never catch up with the horizon. Particles to the right of the black hole horizon travel faster than  $v_{Fl}$ .

In the Corley-Jacobson model, the time-evolution operator is given by

$$U_{CJ}(t) = \mathcal{T} e^{-i \int_0^t dt' \hat{H}_{CJ}(t')}, \quad (58)$$

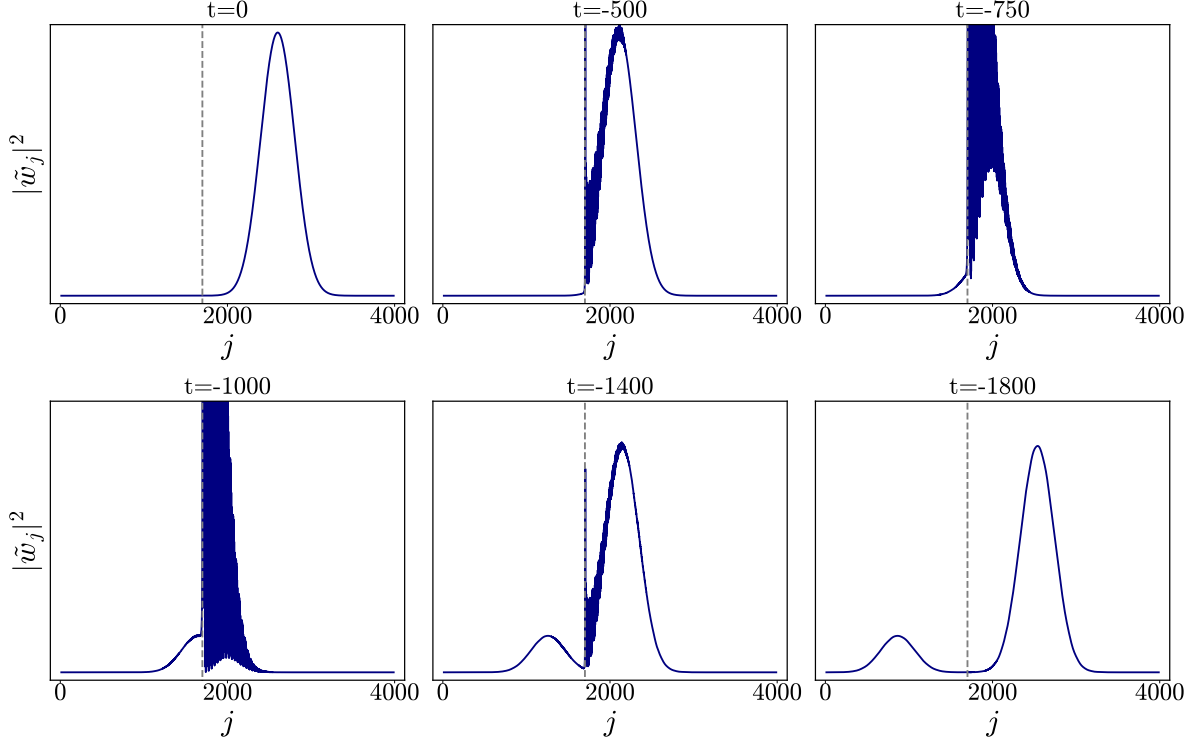


FIG. 9. Backwards-in-time evolution of the wave packet  $W_{x_0, \omega}^\dagger = \sum_j w_j c_j^\dagger$  with  $x_0 = x_b + 900a$  and  $\omega = 0.00298t$ . The width of the wave packet in momentum space is  $\sigma = 0.0025a^{-1}$ . The system size is  $N = 4000$ ,  $x_b = 1700a$  and  $x_w = 3900a$ . The hopping  $t_j$  in Eq. (64) was used with  $\tilde{\kappa} = 0.1$ , together with  $\mu = 0.5t$ .

where  $\mathcal{T}$  is the time-ordering operator. At discrete times  $t = n\Delta t$ , we can write this time-evolution operator as

$$U_{CJ}(n\Delta t) = \mathcal{T} e^{-i \int_{(n-1)\Delta t}^{n\Delta t} dt' \hat{H}_{CJ}(t')} \dots \mathcal{T} e^{-i \int_{\Delta t}^{2\Delta t} dt' \hat{H}_{CJ}(t')} \mathcal{T} e^{-i \int_0^{\Delta t} dt' \hat{H}_{CJ}(t')} \quad (59)$$

Using the following property of the Corley-Jacobson Hamiltonian:

$$\hat{H}_{CJ}(t + \Delta t) = \hat{T}_L^{-1} \hat{H}_{CJ}(t) \hat{T}_L, \quad (60)$$

we can rewrite  $U_{CJ}(n\Delta t)$  as

$$U_{CJ}(n\Delta t) = \hat{T}_L^{-n} \left( \hat{T}_L \mathcal{T} e^{-i \int_0^{\Delta t} dt' \hat{H}_{CJ}(t')} \right)^n \quad (61)$$

$$:= \hat{T}_L^{-n} \tilde{U}(\Delta t)^n \quad (62)$$

$$\approx \hat{T}_L^{-n} U(\Delta t)^n \quad (63)$$

where  $U(\Delta t)$  is the Floquet unitary with a static causal horizon that we used in the main text (Eq. (1)). So we see that there is a close connection between the Corley-Jacobson approach and the Floquet approach. We have checked that quenching  $|\psi_0\rangle$  with either  $\tilde{U}(\Delta t)$  or  $U(\Delta t)$  produces identical results for the Hawking radiation. The additional unitary  $\hat{T}_L^{-n}$  in the Corley-Jacobson time-evolution operator simply implements a transformation from the co-moving frame where the horizon is static to the lab frame where the horizon is moving to the right.

#### D. Details of numerical simulations for the local model

The site-dependent hopping term  $t_j = t(ja)$  used in the local Hamiltonian  $\hat{H}$  is given by

$$t_j/t = 1 - 2S(2\tilde{\kappa}(j - j_b)) - 2S(-2\tilde{\kappa}(j - j_w)) \quad (64)$$

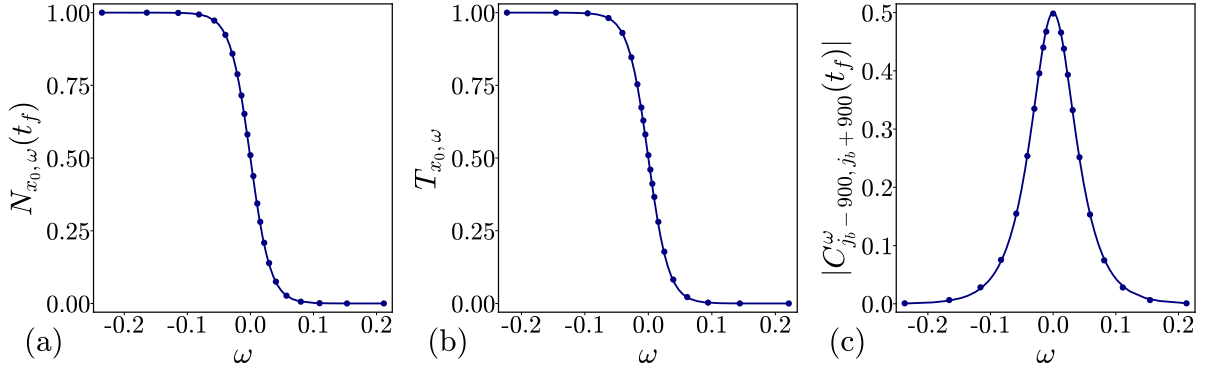


FIG. 10. Numerical results using  $N = 4000$ ,  $j_b = 1700$ ,  $j_w = 3900$  and  $\hat{\kappa} = 0.1$ . (a) Wave packet occupation numbers at time  $t_f$  and position  $j_0 = j_b + 900$  as calculated from (2). (b) Spectrum obtained from the transmission coefficient for right moving wave packets starting at the inside of the horizon  $j_0 = j_b - 900$  (see main text Fig. 6). The results (a) and (b) are nearly identical and coincide perfectly with  $f(\omega)$  (shown by the full line). (c) Wave packet correlation  $|C_{j_b-900, j_b+900}^\omega(t_f)|$  across the horizon with  $t_f = 1850t^{-1}$ , the full line shows  $\sqrt{f(\omega)f(-\omega)}$ .

where  $S(x) = \frac{1}{1+e^x}$ .  $j_b$  ( $j_w$ ) is the location of the black hole (white hole) horizon and  $\hat{\kappa}$  determines the slope of the interpolation between  $t_j = -t$  and  $t_j = t$ , such that the surface gravity is given by  $\kappa = a\partial_x t(x)|_{x=x_b} = \hat{\kappa}t$ .

The wave packet creation operator  $W_{x_0, \omega}^\dagger$  is constructed from the momentum modes of the Minkowski Hamiltonian and is defined as

$$W_{x_0, \omega}^\dagger = \mathcal{N} \sum_{k=-\pi/a}^{k=\pi/a} e^{-(k-k_0)^2/4\sigma^2} e^{-ikx_0} c_k^\dagger, \quad (65)$$

with  $k_0$  a free parameters that determines the momentum mode around which the wave packet is centered (and consequently whether it is left- or right-moving), and  $\sigma$  determines the width of the Gaussian. Here  $c_k^\dagger$  is the (discrete) fourier transform of the on-site creation operators i.e.  $c_k^\dagger = \frac{1}{\sqrt{N}} \sum_{j=1}^N e^{ika_j} c_j^\dagger$ . For all numerical calculations, the width  $\sigma$  was taken to be  $0.0025a^{-1}$  for  $L = 4000a$ , so that the wave packet is as narrow as possible in momentum space, while still able to fit in the inside region in real space. For  $\mu$  we used a value of  $0.5t$ .

Similar to the Floquet case, the time-dependent wave packet occupation number  $N_{x_0, \omega}(t)$  is calculated numerically by transferring the time evolution to the wave packet creation operators  $W_{x_0, \omega}^\dagger$  via  $N_{x_0, \omega}(t) = \langle \psi_0 | W_{x_0, \omega}^\dagger(-t) W_{x_0, \omega}(-t) | \psi_0 \rangle$ , where  $W_{x_0, \omega}^\dagger(-t) = U^\dagger(t) W_{x_0, \omega}^\dagger U(t)$  is the wave packet operator evolved *backwards* in time. An example of a backwards-in-time evolved wave packet is shown in Figure 9. Note that because of the *backwards* time-evolution, the right-moving wave packet actually moves to the left. We see that as time proceeds, the wave packet scatters off the boundary between the inside ( $t_j < 0$ ) and outside ( $t_j > 0$ ) regions, and that only part of it goes through this boundary while the other part is reflected back.

For completeness we also show the time-dependent wave packet occupation number  $N_{x_0, \omega}(t)$ , nearly identical to the Floquet result, and transmission coefficient  $T_{x_0, \omega}$  in Fig. 10.

### E. Hawking radiation via stationary scattering states

Consider the following local quench Hamiltonian used in the main text

$$\hat{H} = \frac{1}{2} \sum_j t_j (ic_{j+1}^\dagger c_j - ic_j^\dagger c_{j+1}) + \mu (c_{j+1}^\dagger c_j + c_j^\dagger c_{j+1}) - 2\mu c_j^\dagger c_j, \quad (66)$$

in the thermodynamic limit  $j \in ]-\infty, +\infty[$ . When  $t_j = t$  is constant the Hamiltonian is readily diagonalised in the fourier basis

$$\hat{H} = \int_{-\pi}^{+\pi} dk [t \sin(k) + \mu \cos(k) - \mu] \hat{b}_k^\dagger \hat{b}_k \quad (67)$$

with  $\hat{b}_k = \frac{1}{\sqrt{2\pi}} \sum_j e^{-ijk} c_j$ . This yields a dispersion relation  $E(k) = t \sin(k) + \mu \cos(k) - \mu$  as shown in Fig. 5 (c). Let us now take  $t_j$  to interpolate between a constant value  $t_{-\infty} = -t$  and  $t_{\infty} = t$ . More precisely we take  $t_{j < j_L} = -t$ ,  $t_{j > j_R} = t$ , and the interpolating region to be within  $[j_L, j_R]$ . For our numerics we used

$$t_j = 1 - \frac{2}{1 + e^{2\tilde{\kappa}j}}. \quad (68)$$

The operators

$$b_E^\dagger = \sum_j f_E(j) c_j^\dagger \quad (69)$$

correspond to single-particle eigenstate creation operators with energy  $E$ , provided that the coefficients  $f_E(j)$  satisfy the following Schrödinger-like equation:

$$\frac{-it_j + \mu}{2} f_E(j+1) + \frac{it_{j-1} + \mu}{2} f_E(j-1) - \mu f_E(j) = E f_E(j) \quad (70)$$

Note that only for  $\mu = 0$  we have a particle hole symmetry,  $f_E^*(j) = f_{-E}(j)$ . One can check that for  $t_j = t$  Eq. (70) indeed reproduces the correct dispersion relation. The discrete Schrödinger equation (70) allows us to define a probability current  $J_j$

$$J_j = \frac{t_j}{2} [f_E^*(j) f_E(j+1) + f_E^*(j+1) f_E(j)] + \frac{i\mu}{2} [f_E^*(j) f_E(j+1) - f_E^*(j+1) f_E(j)], \quad (71)$$

which is conserved, i.e. does not depend on  $j$ :  $J_j = J$ . Eq. (70) can be solved inductively: from  $f_E(j_0 - 1)$  and  $f_E(j_0)$  one can solve for  $f_E(j_0 + 1)$  and subsequently obtain  $f_E(j)$  for general  $j$ .

Eq. (70) will have a solution for every  $E$ , but only for certain  $E$  will the solution be bounded for  $j \rightarrow \pm\infty$ . For a general hopping profile  $t(x)$  interpolating between  $-t$  and  $t$  we anticipate plane wave solutions away from the interpolation region  $j \in [j_L, j_R]$ :

$$f_E(j) = \begin{cases} A_L e^{ik_1 j} + A_R e^{ik_2 j}, & j > j_R \\ B_L e^{iq_1 j} + B_R e^{iq_2 j}, & j < j_L \end{cases} \quad (72)$$

with  $E(k_1) = E(k_2) = E(q_1) = E(q_2)$ . Here  $k_2$  is the momentum of the gapless right-moving mode around  $k = 0$  and  $k_1$  is the momentum of the left-moving mode around  $k_{\text{out}}^*$  (see Fig. 5 (a)). Similarly at the inside of the horizon  $q_1$  is the momentum of the gapless left-moving mode around  $q = 0$  while  $q_2$  is the momentum of the right-moving mode around  $q_{\text{in}}^*$  (see Fig. 5 (b)). Matching the current on both sides via (71) yields (notice that  $k_1 = k_{\text{out}}^* - k_2$ ,  $q_1 = q_{\text{in}}^* - q_2$ , with  $k_{\text{out}}^* = -q_{\text{in}}^* = 2 \arccos(\mu/\sqrt{t^2 + \mu^2})$ ):

$$(t \cos(k_2) - \mu \sin(k_2)) (|A_R|^2 - |A_L|^2) = (-t \cos(q_2) - \mu \sin(q_2)) (|B_R|^2 - |B_L|^2) \quad (73)$$

Inspired by the backwards-in-time evolution of the wave packets as shown in Fig. 9, we are interested in solutions with  $B_L = 0$ ,  $B_R = 1$  and  $q_2 \equiv q_{\text{in}}^* + q$  where  $|q| \ll 1$ , corresponding to right-moving plane waves in the left region  $j < j_L$ . This indeed corresponds to the scattering process of Fig. 9, with a right-moving (left-moving in the backwards-in-time evolution) component on the inside and both a left- and right-moving component on the outside.

We proceed by solving the Schrödinger-like equation numerically starting from the initial values  $f_E(j_L - 1) = e^{iq(j_L - 1)}$  and  $f_E(j_L) = e^{iqj_L}$  and iteratively solving for  $f_E(j)$  until finally arriving at  $f_E(j \geq j_R)$ . The coefficients  $A_L$  and  $A_R$  can then be calculated with

$$A_L = \frac{e^{ik_2} f_E(j_R) - f(j_R + 1)}{e^{ik_1 j_R} (e^{ik_2} - e^{ik_1})} \quad A_R = \frac{e^{ik_1} f_E(j_R) - f(j_R + 1)}{e^{ik_2 j_R} (e^{ik_1} - e^{ik_2})} \quad (74)$$

Notice that from the current conservation Eq.(73) we have (with  $k_2 = q$ ):

$$1 = |A_R|^2 - |A_L|^2, \quad (75)$$

which gives us a nice cross-check on our numerics. The transmission  $T$  and reflection coefficient  $R$  for the backwards-in-time evolution of Fig. 9 are given by

$$T = \frac{1}{|A_R|^2} \quad R = \frac{|A_L|^2}{|A_R|^2} \quad (76)$$

Indeed under backwards-in-time evolution  $A_R$  is the amplitude of the “incoming wave” so that  $B_R$  ( $A_L$ ) is the part that gets transmitted (reflected). The wave packets described in the main text and appendix D are appropriate linear combinations of  $\hat{b}_E^\dagger$ 's such that they are localized in space at  $x_0$  (at  $t = 0$ ) and in energy around some value  $E$ . Since for the initial Minkowski state all negative momentum modes are occupied, and the transmitted part has negative momentum  $q_2$ , while the reflected part has positive momentum  $k_1$ , we can infer the asymptotic occupation number  $N(E)$  of right-moving wave packets outside the horizon (i.e. with amplitude  $A_R$ ) from the reflection coefficient  $T$ :

$$N(E) = \frac{1}{|A_R|^2} \tag{77}$$

which numerically is found to coincide perfectly with the Dirac-Fermi spectrum  $N(E) = 1/(e^{E/k_B T_H} + 1)$  at the Hawking temperature  $T_H$ , in agreement with the results of appendix D.